AMERICAN SOCIETY FOR MICROBIOLOGY | Journal of Virology®

VACCINES AND ANTIVIRAL AGENTS

Broad Sarbecovirus Neutralizing Antibodies Obtained by Computational Design and Synthetic Library Screening

Xuehua Yang,[a] Huarui Duan,[a] Xiuying Liu,[a] Xinhui Zhang,[a] Shengnan Pan,[a] Fangyuan Zhang,[a] Peixiang Gao,[a] Bo Liu,[a] Jian Yang,[a] Xiaojing Chi,[a] Wei Yang[a]

[a]NHC Key Laboratory of Systems Biology of Pathogens, Institute of Pathogen Biology, Chinese Academy of Medical Sciences & Peking Union Medical College, Beijing, China

Xuehua Yang and Huarui Duan contributed equally to this work. Author order is based on research contributions.

ABSTRACT Members of the *Sarbecovirus* subgenus of *Coronaviridae* have twice caused deadly threats to humans. There is increasing concern about the rapid mutation of severe acute respiratory syndrome coronavirus 2 (SARS-CoV-2), which has evolved into multiple generations of epidemic variants in 3 years. Broad neutralizing antibodies are of great importance for pandemic preparedness against SARS-CoV-2 variants and divergent zoonotic sarbecoviruses. Here, we analyzed the structural conservation of the receptor-binding domain (RBD) from representative sarbecoviruses and chose S2H97, a previously reported RBD antibody with ideal breadth and resistance to escape, as a template for computational design to enhance the neutralization activity and spectrum. A total of 35 designs were purified for evaluation. The neutralizing activity of a large proportion of these designs against multiple variants was increased from several to hundreds of times. Molecular dynamics simulation suggested that extra interface contacts and enhanced intermolecular interactions between the RBD and the designed antibodies are established. After light and heavy chain reconstitution, AI-1028, with five complementarity determining regions optimized, showed the best neutralizing activity across all tested sarbecoviruses, including SARS-CoV, multiple SARS-CoV-2 variants, and bat-derived viruses. AI-1028 recognized the same cryptic RBD epitope as the parental prototype antibody. In addition to computational design, chemically synthesized nanobody libraries are also a precious resource for rapid antibody development. By applying distinct RBDs as baits for reciprocal screening, we identified two novel nanobodies with broad activities. These findings provide potential pan-sarbecovirus neutralizing drugs and highlight new pathways to rapidly optimize therapeutic candidates when novel SARS-CoV-2 escape variants or new zoonotic coronaviruses emerge.

IMPORTANCE The subgenus *Sarbecovirus* includes human SARS-CoV, SARS-CoV-2, and hundreds of genetically related bat viruses. The continuous evolution of SARS-CoV-2 has led to the striking evasion of neutralizing antibody (NAb) drugs and convalescent plasma. Antibodies with broad activity across sarbecoviruses would be helpful to combat current SARS-CoV-2 mutations and longer term animal virus spillovers. The study of pan-sarbecovirus NAbs described here is significant for the following reasons. First, we established a structure-based computational pipeline to design and optimize NAbs to obtain more potent and broader neutralizing activity across multiple sarbecoviruses. Second, we screened and identified nanobodies from a highly diversified synthetic library with a broad neutralizing spectrum using an elaborate screening strategy. These methodologies provide guidance for the rapid development of antibody therapeutics against emerging pathogens with highly variable characteristics.

KEYWORDS SARS-CoV-2, pan-sarbecovirus neutralizing antibodies, resistance to escape, computational design, synthetic nanobody library

Editor Kanta Subbarao, The Peter Doherty Institute for Infection and Immunity

Address correspondence to Wei Yang, wyang@ipb.pumc.edu.cn, or Xiaojing Chi, chixiaojing@ipbcams.ac.cn.

The authors declare no conflict of interest.

Received 27 April 2023
Accepted 10 June 2023
Published 27 June 2023

Human coronavirus infections cause common cold, fever, sore throat, pneumonia, and even death (1, 2). The genus *Betacoronavirus* is divided into five subgenera, *Embecovirus*, *Sarbecovirus*, *Merbecovirus*, *Nobecovirus*, and *Hibecovirus* (3, 4). SARS-CoV-2, the pathogen that causes coronavirus disease 2019 (COVID-19), has caused hundreds of millions of infections and killed millions more, becoming one of the worst pandemics in human history. Both severe acute respiratory syndrome coronavirus 2 (SARS-CoV-2) and severe acute respiratory syndrome coronavirus (SARS-CoV) belong to the *Sarbecovirus* subgenus and may have originated from zoonotic spillover and evolved to adapt to human infection (5, 6), which calls for drug stockpiling in case new viruses emerge in the future or to combat ongoing SARS-CoV-2 mutations.

Neutralizing antibodies (NAbs) are an important host defense mechanism that blocks virus entry, and they show clinical benefits in COVID-19 therapeutically and prophylactically (7). Most SARS-CoV-2 NAbs were isolated from convalescent COVID-19 patients, either by antigen-specific single B-cell cloning or by B-cell transcriptome bioinformatics analysis (8 to 10). These methods produce full-human therapeutic NAbs, target diversified binding epitopes, and easily achieve high affinity, but few have broad neutralizing activity. Alternatively, immunized animals, such as mice and llama, can also provide excellent affinity, but the process is slow and involves uncontrolled epitope recognition (11, 12). Therefore, innovative antibody discovery technologies are urgently needed in response to rapid virus evolution.

In addition to SARS-CoV and SARS-CoV-2, bats are known reservoirs of sarbecovirus and high-risk SARS-like strains, such as WIV1, RsSHC014, and RaTG13, which can efficiently use human or bat angiotensin-converting enzyme 2 (ACE2) receptors to enter cells (13, 14). The virus spike protein comprises an S1 subunit that recognizes host cell receptors and an S2 subunit that drives membrane fusion (15). The receptor binding domain (RBD) within the S1 subunit interacts with ACE2 and is the most efficient target for NAbs. A large fraction of immunized polyclonal antibodies and most therapeutic monoclonal antibodies target a subset of epitopes within the receptor binding motif (RBM) that overlap the ACE2-contact surface (16, 17). However, the high amino acid divergences of the RBM among sarbecoviruses have limited the breadth of NAbs and enable ready escape by mutations. To date, several pan-sarbecovirus NAbs have been reported, including sotrovimab (18) (formerly named S309), which recognizes a conserved RBD epitope containing a glycan and is noncompetitive with receptor attachment, S2H97 (19), which binds to a conserved cryptic core RBD epitope with high affinity across all sarbecoviruses, and CR3022 (20), which binds to a distal RBD epitope without clashing with ACE2. Furthermore, S2K146 targets conserved ACE2-binding residues, allowing the antibody to potently inhibit receptor attachment (21). S2E12 and S2M11 competitively block ACE2 attachment, and S2M11 also locks the spike in a closed conformation by the recognition of a quaternary epitope spanning two adjacent RBDs (22). S2X259 (23) and GW01 (24) recognize a highly conserved cryptic epitope of the RBD and cross-react with spikes from multiple clades of sarbecovirus. Antibody 2 - 36 recognizes a region on the "inner side" of the RBD that is buried in the RBD-down conformation of the spike, and blockage of receptor binding likely accounts for neutralization by 2 - 36 (25). Although these conserved epitopes targeting NAbs show a wide neutralization spectrum, their neutralization efficacy varies dramatically.

Computational approaches to antibody design have been promoted by rapid progress in antigen-antibody complex structure analysis, antibody modeling, data-based structure prediction, and deep learning (26 to 29). A structure-based antibody design method has been implemented in the protein modeling program Rosetta and experimentally tested to improve the binding affinity of antibodies against bee hyaluronidase and human immunodeficiency virus gp120 (30). However, high-performance computation-based antibody design still faces a number of technical and theoretical challenges, including inaccurate complementarity determining region (CDR) loop prediction, limited computing power, and massive experimental verification, although it is widely regarded as the future direction of macromolecular drug development.

In addition, synthetic biology has accelerated the application of synthetic antibody libraries, which have played a unique role against infectious diseases (31 to 33). Nanobodies, as

also called single-domain antibodies, are natural monomeric antigen-binding domains from camelid heavy-chain-only antibodies (34). Nanobodies are compact (only ~15 kDa) and can be rapidly produced from microbes such as *Escherichia coli* or yeast cells. SARS-CoV-2 neutralizing nanobodies have been reported by several laboratories, including ours (11, 32, 35 to 37). Since the antigen-binding surface area of nanobodies is smaller than that of conventional antibodies, they are often engineered into multivalent constructs to improve functionality. The classic approach to nanobody discovery is camel- or llama-based animal immunization, which typically takes months and requires a large amount of antigen. We have developed a high-capacity synthetic library-based nanobody screening framework, requiring only 100 μg of antigen and as little as 8 days of screening to obtain binders, making nanobodies a powerful weapon against emerging pathogens (32, 35).

The ongoing mutations of SARS-CoV-2 and the outbreak risk from novel sarbecoviruses highlight the need for broad NAbs. Moreover, rapid iteration methodologies for antibody optimization are undoubtedly desired. In this study, we focused on the design and screening of RBD-targeted pan-sarbecovirus NAbs by using integrated computational approaches and rapid biopanning with a synthetic nanobody library. These designed full-human antibodies and screened nanobodies showed optimal neutralizing activity and breadth. These new paradigms for antibody discovery will enhance our control capability against infectious diseases.

RESULTS

Sarbecovirus sequence similarity mapped onto the RBD surface. Sarbecovirus RBD mediates contact with entry receptors. For SARS-CoV-2, highly potent NAbs usually recognize epitopes within the RBD but exhibit limited cross-reactivity for emerging variants. To identify possible epitopes for pan-sarbecovirus NAbs, we used the ConSurf program to map conserved residues on the structure of the RBD (30). The sequences used for alignment and evolutionary conservation visualization are based on the evolution and receptor usage by sarbecoviruses (38) and were obtained from 20 representative SARS-CoV-2 isolates (Fig. 1A), as well as more than 30 sarbecoviruses (Fig. 1B). The RBD was structurally categorized by a global consortium study into seven "core" antibody-binding communities (39). As shown in Fig. 1A and B, communities RBD-1 through RBD-4 overlap the RBM and are highly variable, suggesting that they are susceptible to neutralization escape, although the NAbs recognizing these communities are mostly potent against sensitive isolates. Therefore, antibodies targeting communities RBD-1 through RBD-4 have little chance to elicit pan-sarbecovirus activities. NAbs binding to RBD-5 through RBD-7 are more resistant to escape for SARS-CoV-2 variants (Fig. 1A). In contrast, only RBD-6 and part of RBD-7, previously described as a cryptic epitope on the inner face of the RBD, are conserved among all analyzed sarbecoviruses (Fig. 1B), providing an optimal binding target for broad-spectrum NAbs.

The multisequence alignment of representative RBD sequences is shown in Fig. 1C with the Wuhan-Hu-1 isolate as the parental sequence and the mutated sites labeled in each variant. In general, SARS-CoV-2 variants accumulate increasing mutations as the pandemic continues. The Omicron BA.5 variant has 17 mutation sites in the RBD alone. Notably, the RBD homology between SARS-CoV and SARS-CoV-2 (Wuhan-Hu-1) is only 73.5%, with a highly variable region located on the RBM. These analyses suggest that it is quite difficult to obtain pan-sarbecovirus NAbs through infection or vaccination, and the RBD-6 community may be an ideal epitope due to its natural conservative characteristics.

Computational design and optimization of RBD-6 antibodies. Rapid antibody design methods are urgently needed as powerful tools to combat SARS-CoV-2 evolution. To optimize RBD-6 binding antibodies against emerging variants, we first sought to choose an experimentally identified pan-sarbecovirus NAb as the prototype for computational design. Starr and colleagues (19) described a human monoclonal antibody (S2H97) that neutralizes a broad range of sarbecoviruses, including both 2003 SARS-CoV and SARS-CoV-2. However, its activity fluctuated near the level of 1 μg/mL, which still has great potential for optimization. As shown in Fig. 2A, the S2H97 antibody targets a cryptic antigenic site located near RBD-6 (PDB 7M7W), making it a good example for optimization to be more potent against multiple sarbecoviruses. To test this scenario, we established an integrated structure-based antibody design framework with the aid of RosettaAntibodyDesign (RAbD) (40). The S2H97

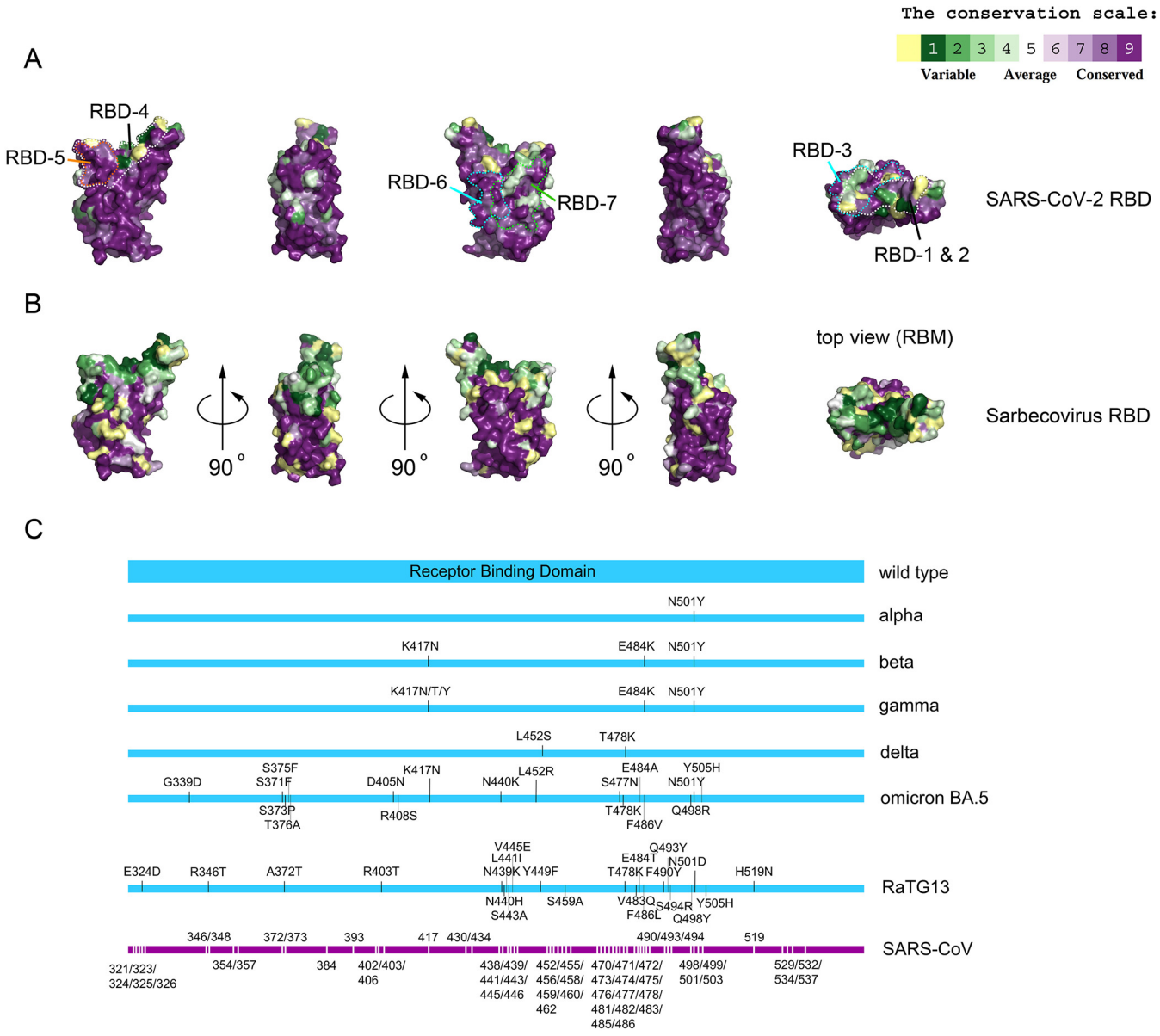

FIG 1 Amino acid conservation mapped onto the structure of the RBD. (A) The conservation pattern of SARS-CoV-2 RBDs. Using the ConSurf server and 20 representative SARS-CoV-2 RBD sequences (Wuhan-Hu-1, Alpha, Beta, Gamma, Delta, Lambda, Kappa, Epsilon, Eta, Iota, Zeta, Omicron-BA.1, BA.2, BA.4, BA.5, BF.7, BQ.1.1, CA.3.1, CH.1.1, and XBB), each residue was colored from 1 (most variable, green) to 9 (most conserved, purple) and mapped onto the surface. Yellow areas represent missing amino acids. (B) The conservation pattern of sarbecovirus RBDs. The same ConSurf analysis was performed using more than 30 sarbecovirus RBDs (SARS-COV Tor2, WIV1, HKU3-1, RsSHC014, Rc-0319, GX-P4L, RaTG13, bat SARS-like coronavirus RsSHC014, YNLF_34C, Rs9401, SL_CoVZXC21, and SARS-COV-2 isolates as described in Fig. 1A). (C) Maps of RBD mutations for representative SARS-CoV-2 variants, bat RaTG13 and SARS-CoV by alignment with the Wuhan-Hu-1 isolate as the wild type.

affinity is dominated by interactions of the heavy chain CDR3 (HCDR3) with an RBD crevice at the center of a consensus epitope, together with polar contacts with HCDR1, HCDR2, and LCDR2 (19). For computational design, with this knowledge, we designed a light chain or heavy chain. All LCDR1, LCDR2, and LCDR3 or HCDR1 and HCDR2 in S2H97 were designed for graft and sequence sampling, allowing new lengths and clusters in the final designed antibodies. The residues in HCDR3 and the framework held their starting amino acid identities for maximal retention of affinity. The final antibody form consisted of either the wild-type heavy chain combined with the designed light chains or the designed heavy chains combined with the wild-type light chain. As shown in Fig. 2B and C, based on a ranking of the physical characteristics of each design generated by the computation reports, we chose 15 designed light chains and 20 designed heavy chains for full antibody expression and purification. The change in Rosetta energy, the solvent-accessible area buried at the interface, and the total

A

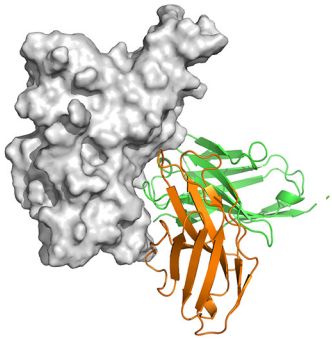

B

Ab name	L-CDR1	L-CDR2	L-CDR3
S2H97	TGISSDVGGYNSVS	DVTNRPS	SSYTSSSTP--PYV
AI-2	SGSS-SDIGNNSVN	DVTNRPS	GAYDSSLD--KEFV
AI-3	SG---NNIGTKYAH	DVTNRPS	GGHDSSLD--HEYL
AI-4	SGSD-SNIGRRSVN	DVTNRPS	SGHDSSLD--HEYS
AI-5	VMG--DSQGNYNLS	DVTNRPS	GGFDSSLD--QEFT
AI-6	GSSTGAVTSGNYAN	DVTNRPS	SASKIVNKK-YVYT
AI-7	TRSSGNIAS-NYVQ	DVTNRPS	AASSNIRES-YVFV
AI-8	TGTSNDIGAHDLVS	QGTYLPE	AAYDSSLG---GYV
AI-9	TGSK-SDIGSSYVS	QGTLIPA	AAYDTSLN---MFV
AI-10	TGTSSDIGASDLVS	DTTLVPA	ATFEMDME--NKYL
AI-11	TGTSSDIGAYDHVS	DGSYLPA	AALTSS---D-TYV
AI-12	TGTSNDIGAYDFVS	DTSYVPA	LAYDRSLN---GYV
AI-13	TGSSSDIG-KSYVS	DTSYLPA	AVATVVNGTY-IYT
AI-14	RSSSGSITSSNYAS	HGTYIPA	AAWDSSLN---AYV
AI-15	TGTSSDIGSYDYVS	DTSYLPA	ASHSSS-LDY-KYI
AI-16	SG---DNLGDKLVS	DDTYLPA	ATFEKDLD--NKYV

C

Ab name	H-CDR1	H-CDR2
S2H97	KGSGYSFTSYWIG	IIYPGDSDTR
AI-18	TVSGAAFHTYWIA	MIFPGYGDTR
AI-19	TGDGYAFKEYWIA	MIFPGYGDTR
AI-20	TGDGYAFEMYWIA	MIFPGQGDTR
AI-21	TGDGYAFKEYWIA	MIFPGQGDTR
AI-22	TGSGYAFKEYWIA	MIYPGQNDTR
AI-23	TGSGYAFKEYWIA	MIFPGQNDTR
AI-24	TGSGYAFKEYWIA	MIFPGQGDTR
AI-25	TGTGYAFLMYWIA	QIFPGQGDTI
AI-26	TGSGYAFKEYWIA	QIFPGQNDTI
AI-27	TGDGYVFQAYWIS	RIFPGQGDTE
AI-28	TGTGYVFKAYWIS	RIYPGQGDTE
AI-29	TGSGYAFKEYWIS	RIYPGQNDTE
AI-30	TGTGYAFKEYWIA	MIYPGQGDTR
AI-31	TGTGYNFKEYWIA	MIYPGQGDTR
AI-32	TGSGYAFKEYWIA	MIYPGQGDTR
AI-33	TGDGYAFKEYWIA	MIYPGQGDTV
AI-34	TGSGYAFKEYWIA	MIYPGQGDTV
AI-35	TGDGYKFTEYWIA	MIYPGQGDTR
AI-36	TGDGYKFNEYWIA	MIYPGQGDTV
AI-37	TGDGYAFKEYWIA	MIYPGQGDTR

D

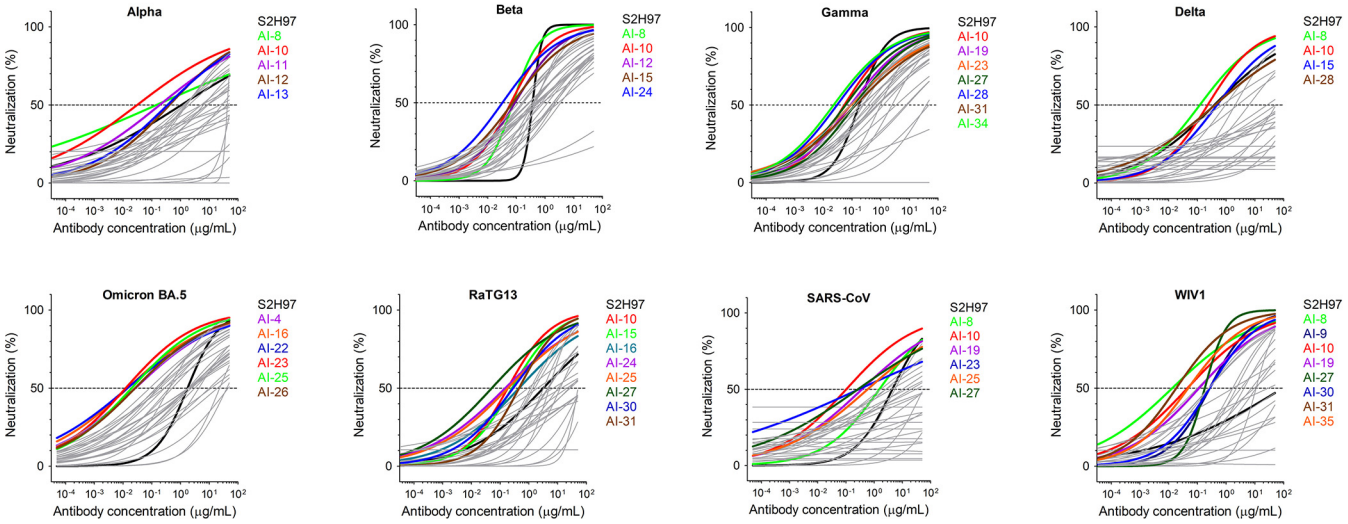

FIG 2 Computational design and neutralizing activity of the RBD-6 antibodies. (A) Schematic representation of the binding orientation of the S2H97 Fab fragment on the RBD, with the light chain colored orange and heavy chain colored green. (B) Amino acid sequences of designed light chain CDRs. Background color with yellow for identical residues, cyan for conservative, and green for block of similar. (C) Amino acid sequences of the designed heavy chains CDR1 and CDR2. (D) Pseudoviruses were packaged with particular Spike proteins derived from SARS-CoV-2 variants Alpha, Beta, Gamma, Delta, Omicron BA.5, bat CoV RaTG13, 2003 SARS-CoV, and bat CoV WIV1. Fitted neutralization curves were determined by the parental S2H97 and 35 designed antibodies. The antibodies with improved potency are emphasized with colors. The experiments were performed independently at least twice and similar results were obtained. The results of one representative experiment are shown, and the data are the average values of three replicates (n = 3).

cross-interface hydrogen bonds were the main considerations in candidate selection (Table S1 in the supplemental material). The parental S2H97 and designed antibodies showed satisfactory yields without detectable aggregation (Fig. S1 and 2).

To fully interrogate the breadth of the designed antibodies, we assessed the neutralizing potency of the prototype and designed antibodies (named AI-antibody) against a panel of envelope pseudotyped viruses, including SARS-CoV-2 variants Alpha, Beta, Gamma, Delta, Omicron subvariant BA.5, and SARS-CoV, as well as bat coronavirus RaTG13 and WIV1 (Fig. 2D). The antibody concentration at 50% neutralization (NT_{50}) is summarized in Table 1. We set the NT_{50} of S2H97 as the reference and then compared whether the neutralizing activity of these designed antibodies was improved against specific viruses. Notably, for each tested virus, there were always several candidates with improved neutralizing activity compared with S2H97. The increase ranged from several to hundreds of times. For example, the NT_{50} value was 0.01 μg/mL for AI-23 versus 1.76 μg/mL for S2H97 against Omicron BA.5 and 0.10 μg/mL for AI-10 versus 4.45 μg/mL for S2H97 against SARS-CoV. AI-8, AI-10, AI-23, and AI-25 showed satisfactory overall performance, with significant improvement in neutralization potency.

TABLE 1 Neutralizing activity of the prototype and designed antibodies against representative pseudoviruses[a]

	Alpha		Beta		Gamma		Delta		BA.5		RaTG13		SARS		WIV1	
	μg/mL	nM	μg/mL	nM	μg/mL	nM	μg/mL	nM	μg/mL	nM	μg/mL	nM	μg/mL	nM	μg/mL	nM
S2H97	1.08	7.19	0.37	2.45	0.18	1.18	0.39	2.61	1.76	11.76	3.18	21.20	4.45	29.69	94.76	>300
2	ND	ND	0.41	2.73	48.15	>300	ND	ND	0.28	1.87	1.16	7.73	30.78	205.20	>50	>300
3	>50	>300	0.43	2.84	0.80	5.36	>50	>300	0.14	0.92	4.52	30.14	5.47	36.49	>50	>300
4	>50	>300	0.48	3.20	2.49	16.59	>50	>300	0.03	0.18	5.11	34.05	>50	>300	>50	>300
5	8.41	56.05	0.54	3.59	8.44	56.25	>50	>300	0.14	0.94	>50	>300	>50	>300	11.05	73.67
7	>50	>300	>50	>300	>50	>300	>50	>300	0.08	0.56	>50	>300	>50	>300	>50	>300
8	0.15	0.97	0.08	0.51	0.98	6.54	0.12	0.81	2.41	16.06	>50	>300	1.54	10.26	0.01	0.09
9	5.42	36.13	0.29	1.92	7.65	51.01	>50	>300	1.87	12.44	10.50	70.00	>50	>300	0.27	1.79
10	0.03	0.21	0.06	0.43	0.05	0.36	0.23	1.53	10.05	67.00	0.18	1.23	0.10	0.69	0.05	0.30
11	0.19	1.26	0.60	3.99	3.47	23.13	>50	>300	2.04	13.59	>50	>300	>50	>300	0.10	0.67
12	0.41	2.76	0.09	0.59	0.36	2.39	2.07	13.81	3.13	20.86	21.29	141.93	20.57	137.13	7.66	51.09
13	0.35	2.36	2.93	19.55	39.12	260.80	>50	>300	0.20	1.30	0.93	6.20	1.74	11.57	>50	>300
14	>50	>300	>50	>300	>50	>300	>50	>300	0.27	1.80	>50	>300	>50	>300	>50	>300
15	1.28	8.54	0.07	0.49	0.25	1.64	0.48	3.23	0.16	1.08	0.26	1.73	>50	>300	>50	>300
16	43.37	289.13	0.39	2.57	0.08	0.57	0.95	6.30	0.01	0.10	0.45	3.03	>50	>300	>50	>300
18	1.62	10.78	1.99	13.25	0.24	1.61	6.25	41.68	46.11	>300	27.59	183.93	10.16	67.73	>50	>300
19	>50	>300	ND	ND	0.09	0.59	ND	>300	0.52	3.45	>50	>300	0.37	2.48	0.11	0.76
20	27.74	184.93	3.51	23.37	0.09	0.61	>50	>300	0.16	1.09	2.01	13.42	>50	>300	2.27	15.11
21	1.38	9.23	1.89	12.58	0.21	1.42	>50	>300	19.28	128.53	4.86	32.38	>50	>300	29.43	196.20
22	1.97	13.14	2.38	15.84	0.59	3.95	26.71	178.07	0.01	0.09	>50	>300	4.18	27.88	>50	>300
23	>50	>300	2.24	14.95	0.09	0.62	>50	>300	0.01	0.08	>50	>300	0.29	1.94	1.70	11.30
24	5.27	35.15	0.03	0.22	0.74	4.93	>50	>300	0.03	0.17	0.15	1.01	>50	>300	>50	>300
25	>50	>300	0.16	1.05	0.45	3.01	2.52	16.80	0.02	0.13	0.19	1.24	0.59	3.96	1.75	11.67
26	>50	>300	0.51	3.42	0.82	5.50	>50	>300	0.03	0.18	13.52	90.13	2.60	17.36	>50	>300
27	1.48	9.89	0.27	1.79	0.06	0.40	0.73	4.85	1.98	13.20	0.05	0.34	0.27	1.78	0.18	1.21
28	>50	>300	0.18	1.18	0.03	0.20	0.41	2.73	11.76	78.40	7.05	47.02	2.67	17.81	4.20	27.99
29	1.66	11.09	0.89	5.91	0.18	1.20	>50	>300	1.84	12.26	>50	>300	>50	>300	0.25	1.70
30	9.11	60.72	0.12	0.78	0.54	3.61	>50	>300	23.16	154.40	0.28	1.89	>50	>300	0.27	1.78
31	>50	>300	0.46	3.07	0.13	0.89	>50	>300	2.30	15.36	0.46	3.04	>50	>300	0.02	0.12
32	>50	>300	0.74	4.90	0.12	0.82	>50	>300	1.93	12.83	12.38	82.53	>50	>300	0.25	1.67
33	6.37	42.45	0.16	1.07	0.13	0.84	>50	>300	0.40	2.69	1.36	9.07	13.91	92.73	0.25	1.66
34	>50	>300	0.36	2.39	0.02	0.15	>50	>300	1.92	12.81	1.61	10.76	>50	>300	9.54	63.61
35	>50	>300	0.79	5.24	1.24	8.28	>50	>300	40.97	273.13	3.26	21.70	>50	>300	0.05	0.32
36	23.82	158.80	1.23	8.17	0.09	0.59	>50	>300	4.33	28.86	>50	>300	>50	>300	11.09	73.93
37	8.72	58.13	0.40	2.67	0.77	5.16	>50	>300	0.40	2.67	25.51	170.07	>50	>300	3.29	21.95

[a]NT_{50} values are indicated in both μg/mL and nM. ND, not detected.

We further determined the equilibrium binding affinity (K_D) of the selected antibodies by surface plasmon resonance (SPR) using representative recombinant RBD proteins from Alpha, Omicron BA.5, and SARS-CoV (Fig. 3). Both S2H97 and the designed antibodies showed cross-reactive binding to all tested RBDs with K_D values ranging from 1.34 to <0.001 nM. Notably, all these antibodies exhibited extremely high affinity with a very low dissociation constant (K_d), suggesting a longer binding half-life and higher binding stability in serum. We also noted that although the neutralizing activity of these designed antibodies was significantly improved, their binding affinity was comparable, indicating that S2H97 and its derived antibodies belong to a class of antibodies with an inherent strong affinity to their target (19).

When the affinity constant reaches or approaches the limit of SPR detection, the imperceptible binding affinity difference may not contribute to the change in neutralizing activity. These data signify that biological computing systems can be efficiently used for SARS-CoV-2 NAb optimization and maturation.

Structural analysis of the designed antibodies. To further investigate why these designs showed improved neutralizing activity from a structural perspective, we analyzed antigen-antibody complex structures deduced from RAbD calculations. As shown in Fig. 4A, the interface between the parental S2H97 and RBD could be characterized by several features. First, the interaction area is relatively extensive with the involvement of all three heavy-chain CDRs and LCDR2. Second, the HCDR3 loop plays a key role by partially inserting into an RBD crevice at the center of the epitope. Third, the RBD amino acids participating in

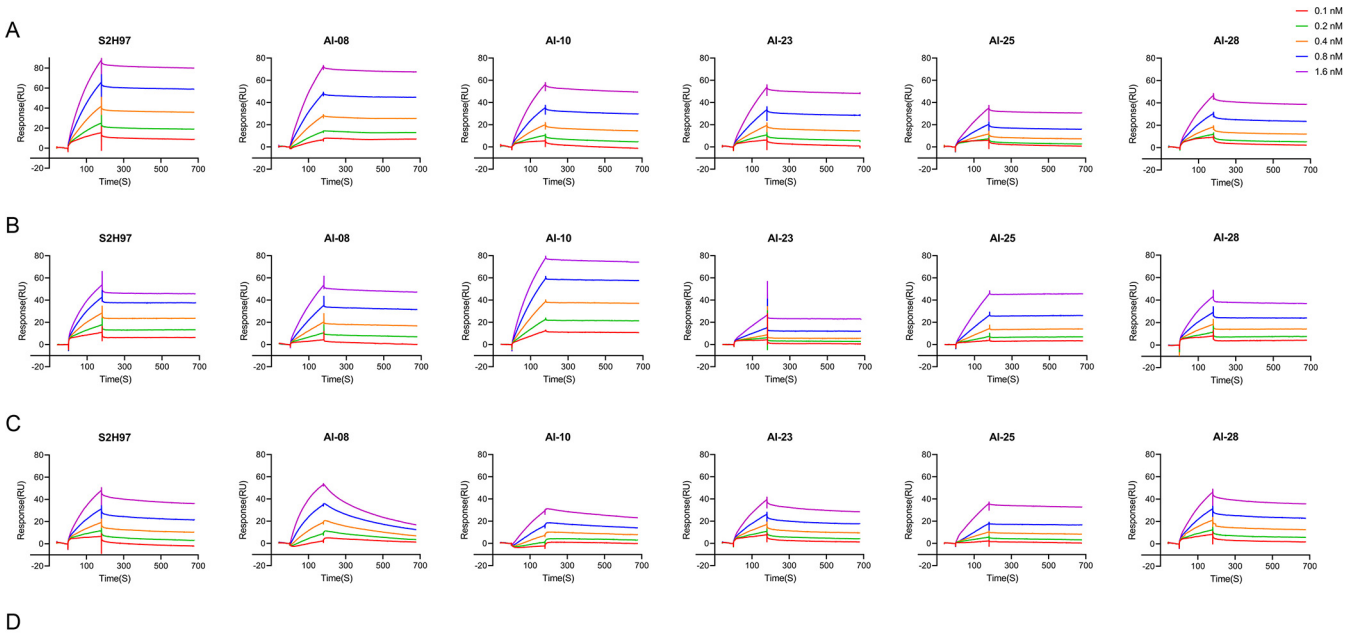

D

	S2H97			AI-8			AI-10			AI-23			AI-25			AI-28		
	*K*a (1/Ms)	*K*d (1/s)	*K*D (M)	*K*a (1/Ms)	*K*d (1/s)	*K*D (M)	*K*a (1/Ms)	*K*d (1/s)	*K*D (M)	*K*a (1/Ms)	*K*d (1/s)	*K*D (M)	*K*a (1/Ms)	*K*d (1/s)	*K*D (M)	*K*a (1/Ms)	*K*d (1/s)	*K*D (M)
Alpha	9.75×10^{6}	1.08×10^{-4}	1.11×10^{-11}	7.24×10^{6}	1.18×10^{-4}	1.64×10^{-11}	1.21×10^{7}	4.23×10^{-4}	3.49×10^{-11}	4.92×10^{6}	2.99×10^{-4}	6.07×10^{-11}	4.97×10^{6}	1.85×10^{-4}	3.72×10^{-11}	7.44×10^{6}	3.51×10^{-4}	4.71×10^{-11}
Omicron BA.5	1.54×10^{7}	3.89×10^{-5}	2.53×10^{-12}	4.35×10^{7}	2.28×10^{-4}	5.24×10^{-12}	8.54×10^{6}	5.31×10^{-5}	6.22×10^{-12}	8.94×10^{6}	2.27×10^{-7}	2.54×10^{-13}	3.24×10^{6}	1.06×10^{-7}	3.27×10^{-14}	4.29×10^{6}	5.98×10^{-5}	1.39×10^{-11}
SARS-CoV	6.10×10^{6}	7.37×10^{-4}	1.21×10^{-11}	2.73×10^{6}	3.66×10^{-3}	1.34×10^{-9}	2.28×10^{6}	7.40×10^{-4}	3.25×10^{-10}	8.38×10^{5}	5.07×10^{-4}	6.05×10^{-10}	1.75×10^{7}	1.39×10^{-4}	7.94×10^{-12}	6.03×10^{6}	4.40×10^{-4}	7.31×10^{-11}

FIG 3 Binding affinity of S2H97 and designed antibodies to the representative RBDs. Fitted line plot showing the binding kinetics of NAbs with the immobilized RBD proteins, measured using surface plasmon resonance (SPR). Recombinant RBD proteins were derived from SARS-CoV-2 variants Alpha (A), Omicron BA.5 (B), and SARS-CoV (C). The antibody concentrations are shown in different colors. (D) Summary of SPR kinetic and affinity measurements. The equilibrium dissociation constant (K_D), the association rate (K_a), and the dissociation rate (K_d) are presented. RU, relative units.

polar interactions are basically conserved, including sarbecovirus-conserved R357, D428, S514, and E516, as well as SARS-CoV-2-conserved K462 (Fig. 4A and F). Overall, the designed antibodies exhibited more polar interactions after CDR sequence and length optimization, probably helping to stabilize the antigen-antibody complex. In detail, some new interactions were observed in AI-8 for LCDR2 Y69/N360 and LCDR2 E72/H519 (Fig. 4B); in AI-23 for HCDR1 K37/D427, HCDR1 E38/D427, HCDR2 Q65/N460, and LCDR2 S72/H519 (Fig. 4D); and in AI-25 for HCDR2 Q65/N460 and LCDR2 S72/H519 (Fig. 4E). Interestingly, although the neutralization activity of AI-10 was significantly improved, the structural analysis did not find an increasing trend of polar interactions represented by hydrogen bonds (Fig. 4C), suggesting other enhancement mechanisms. RBD conservation analysis revealed that some newly generated interaction key sites (N360 and D427) are extremely highly conserved among sarbecoviruses, while other amino acids (N460 and H519) are completely identical in variants of SARS-CoV-2 (Fig. 4F).

Generation and validation of pan-sarbecovirus AI-1028. To preserve the neutralizing activity from the parental S2H97 as much as possible, we conservatively designed only either the light chain or heavy chain in the first-round calculation. However, we always found variant-specific escape, such as Omicron BA.5 escaping from AI-10, Alpha from AI-25, and even WIV1 from the parental S2H97 (Table 1), making these designs less than ideal. Therefore, we reconstituted new antibodies by combining selected light chains with heavy chains and evaluated their activity (Table S2). AI-1028 was derived from the AI-10 light chain combined with the AI-28 heavy chain and exhibited the best performance. As shown in Fig. 5A, eight representative pseudotyped sarbecoviruses were prepared for the neutralization assay. We found that AI-1028 broadly neutralized all pseudoviral variants with improved NT_{50}, ranging from 0.01 to 1.96 μg/mL (equivalent to 0.08 to 13 nM). Notably, the activity for both Omicron BA.5 and SARS-CoV reached very low NT_{50} values, suggesting potential application prospects. We further measured the binding kinetics of AI-1028 against representative RBDs by SPR. AI-1028 demonstrated strong affinity to all tested RBDs with K_D values of approximately 10^{-11} M

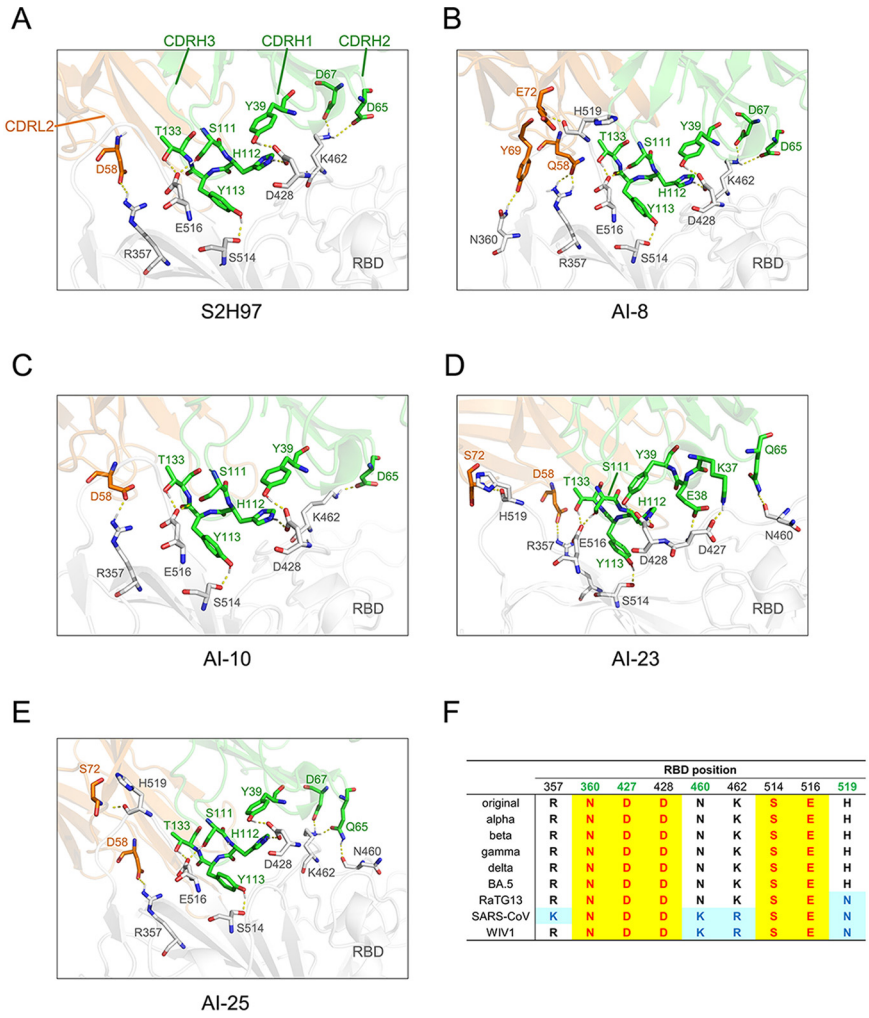

F

	RBD position								
	357	360	427	428	460	462	514	516	519
original	R	N	D	D	N	K	S	E	H
alpha	R	N	D	D	N	K	S	E	H
beta	R	N	D	D	N	K	S	E	H
gamma	R	N	D	D	N	K	S	E	H
delta	R	N	D	D	N	K	S	E	H
BA.5	R	N	D	D	N	K	S	E	H
RaTG13	R	N	D	D	N	K	S	E	N
SARS-CoV	K	N	D	D	K	R	S	E	N
WIV1	R	N	D	D	K	R	S	E	N

FIG 4 Predicted structure of important interface interactions on optimized antibodies. Zoomed in view of the predicted structure of interactions between the parental antibody S2H97 (A) or optimized antibodies AI-8 (B), AI-10 (C), AI-23 (D), and AI-25 (E) with related residues on RBD (gray). The heavy chain is labeled in green, and the light chain is labeled in tan. Hydrogen bonds are indicated by the yellow dotted line. (F) Conservation analysis of key interacting amino acid sites.

(Fig. 5B). To test whether AI-1028 and the parental S2H97 share the same binding epitope, we performed an in-tandem SPR-based binding assay. S2H97 bound to the RBD and blocked the subsequent binding of AI-1028. In contrast, prebinding of the RBD by an isotype IgG control did not abolish the subsequent binding of AI-1028 (Fig. 5C). To further evaluate the neutralizing spectrum of AI-1028, we prepared pseudoviruses from the latest Omicron variants XBB, BQ.1.1 and BA.2.3.20, which are becoming the dominant variants in some countries and show resistance to existing NAbs. Encouragingly, AI-1028 demonstrated better neutralizing activity than its design template S2H97, with an increased activity of 3.7-fold against XBB, 9.5-fold against BQ.1.1, and 7.3-fold against BA.2.3.20 (Fig. 5D). These results indicate that AI-1028 is a successfully designed example with optimal performance.

Pan-sarbecovirus nanobody screen from a synthetic library. Nanobodies are attractive drug candidates for the prevention and treatment of COVID-19 because of their low cost and high stability (11, 32, 36, 41). We previously described an ultrapotent pan-SARS-CoV-2 neutralizing nanobody identified by screening a synthetic nanobody library (35). However, it failed to bind to other sarbecoviruses, such as SARS-CoV. In this study, we designed a strategy with four-round alternate biopanning by using RBD antigens from Alpha or Omicron BA.5 variants as the baits for the first and third rounds of binding and SARS-CoV RBD as the bait for the second and fourth rounds of binding, as illustrated in Fig. 6A. This strategy maximized the possibility of hits recognizing conserved epitopes. After four rounds of

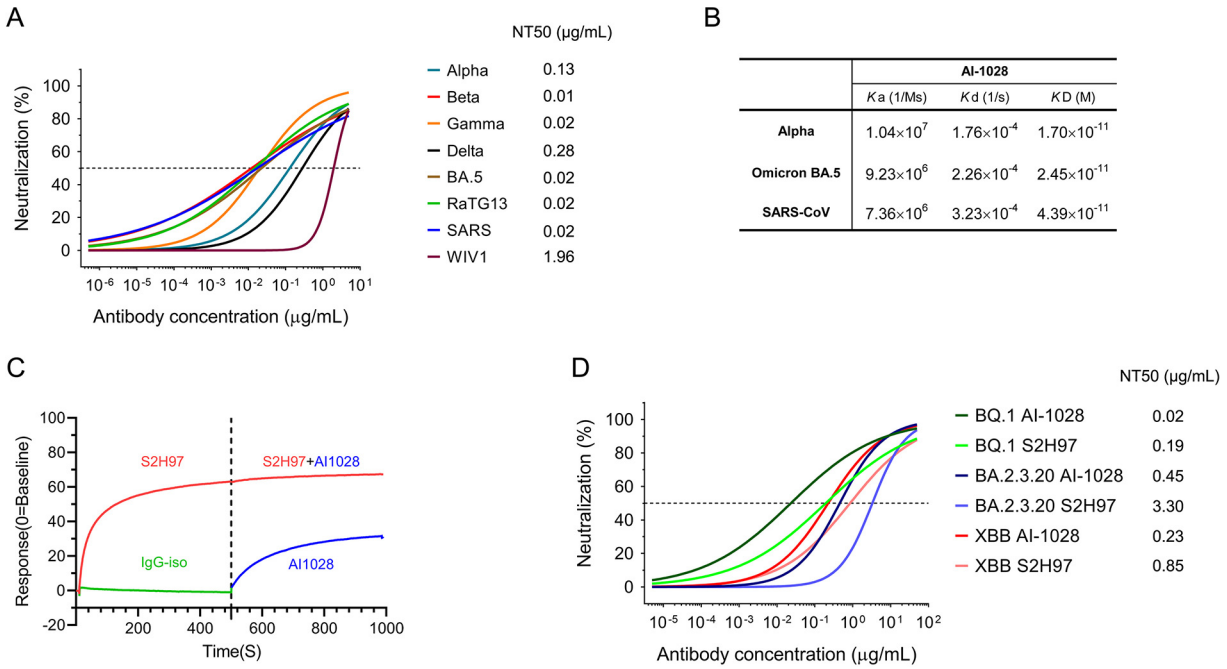

FIG 5 Generation and validation of pan-sarbecovirus NAb AI-1028. (A) AI-1028 neutralizing curves and NT_{50} values from eight pseudotyped viruses displaying the spike proteins as indicated. The experiments were performed independently at least twice and similar results were obtained. The results of one representative experiment are shown, and the data are the average values of three replicates (n = 3). (B) Summary of AI-1028 binding kinetic and affinity measurements to the indicated RBDs. (C) The epitope preblocking effects using S2H97 (red) or an isotype IgG (green) as the first antibody and AI-1028 as the second antibody. The segments of each sensorgram are color coded to show individual binding events. (D) Neutralization comparison between S2H97 and AI-1028 against Omicron subvariants BQ.1.1, BA.2.3.20, and XBB.

biopanning, five independent nanobodies were obtained. To determine the potential neutralization breadth of these nanobodies, we generated a panel of SARS-CoV-2 pseudoviruses bearing point mutations in the spike gene (Table 2). Nb-10 showed the most extensive mutation resistance with potential interacting residues around K378 and F377. In contrast, other nanobodies more easily escaped (Table 2). To obtain more nanobody hits, we added a fifth round of panning with BA.5 RBD as bait, but only one clone was enriched and designated Nb-09. However, the monovalent Nb-09 showed weak neutralizing potency (Fig. S3). Finally, two nanobodies were chosen and expressed in either bivalent (Bi-09) or monovalent (Nb-10) forms (Fig. 6B) for further evaluation. The amino acid sequences of both nanobodies are shown in Table S5.

A total of 10 representative pseudoviruses were used to assess the neutralization breadth of both nanobodies. Bi-09 could neutralize all tested pseudoviruses with NT_{50} values ranging from 0.06 to 42.72 μg/mL, although relatively weak activity against XBB, Delta, and WIV1 was observed (Fig. 6C). Compared to the Bi-09 nanobody, Nb-10 retained good neutralizing activity toward the majority of tested pseudoviruses, including Omicron variants, with the exception of BA.5. (Fig. 6D). The equilibrium-binding affinities are summarized in Fig. 6E, showing a consistent trend in their neutralizing activities. The neutralizing activity of nanobodies against different isolates varies greatly. This may be because the antigen-nanobody interface is more limited than that of conventional antibodies, making them more susceptible to RBD mutations. Taken together, our results indicate that pan-sarbecovirus NAbs can be rapidly prepared through high-performance biological computation and guided synthetic library screening.

DISCUSSION

In this article, we report the exploration of pan-sarbecovirus NAbs by computational design to obtain more potent and broader neutralizing activity against multiple sarbecoviruses. For a particular virus isolate, computational designs could efficiently increase neutralization activity by several to hundreds of times compared to that of the original prototype antibody. Structural prediction suggested that this increase was associated

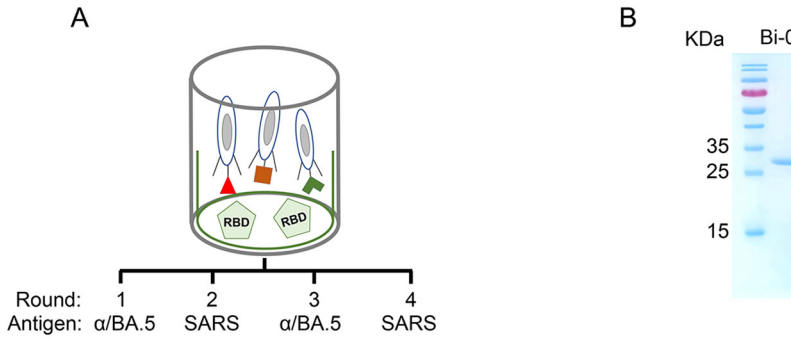

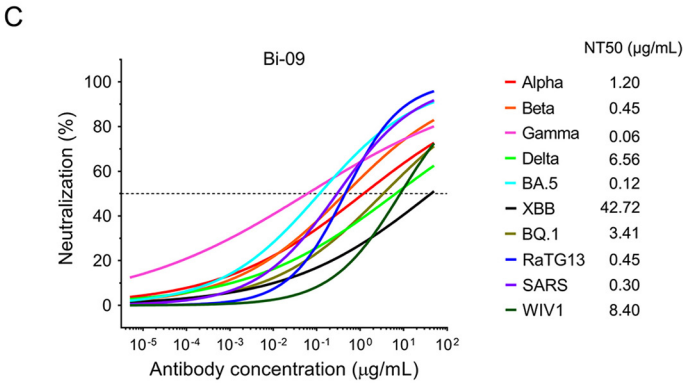

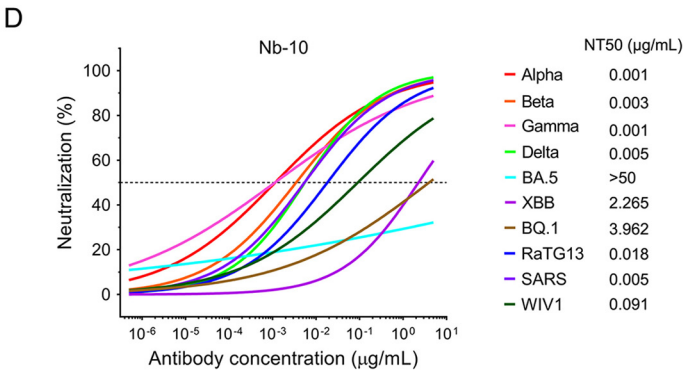

E

	Bi-09			Nb-10		
	*K*a (1/Ms)	*K*d (1/s)	*K*D (M)	*K*a (1/Ms)	*K*d (1/s)	*K*D (M)
Alpha	2.86×10^{5}	3.65×10^{-3}	1.29×10^{-8}	1.65×10^{5}	2.73×10^{-4}	1.65×10^{-9}
Omicron BA.5	6.25×10^{5}	1.24×10^{-3}	1.88×10^{-9}	7.43×10^{3}	0.65	8.75×10^{-5}
SARS-CoV	3.49×10^{5}	5.10×10^{-4}	1.46×10^{-9}	4.62×10^{4}	8.56×10^{-4}	1.85×10^{-8}

FIG 6 Pan-sarbecovirus nanobody screen from a synthetic library. (A) Schematics for broad nanobody screening from a synthetic phage display library. Recombinant RBD proteins from the indicated viruses are used as antigens. (B) The purified recombinant nanobodies were separated by SDS-PAGE and stained with Coomassie blue. (C and D) Neutralizing curves and NT_{50} values of Bi-09 (C) and Nb-10 (D) against 10 pseudotyped viruses. (E) Summary of nanobody binding kinetic and affinity measurements to the indicated RBDs.

with increased numbers of interface interactions. By recombining the designed light and heavy chains, we identified a novel antibody, AI-1028, with the best neutralizing activity against all SARS-CoV-2 variants we tested, including recent Omicron subvariants XBB, BQ.1.1, and BA.2.3.20. Remarkably, AI-1028 also effectively neutralized SARS-CoV, bat coronavirus RaTG13, and WIV1. For an alternative approach, we also identified nanobodies from a synthetic antibody library with a broad neutralizing spectrum using a screening strategy against multiple RBD variants designed to select for nanobodies targeting conserved epitopes with

TABLE 2 NT_{50} values of the indicated nanobodies against SARS-CoV-2 mutation pseudovirus[a]

Mutations	Nb-01	Nb-02	Nb-06	Nb-07	Nb-10	Mutations	Nb-01	Nb-02	Nb-06	Nb-07	Nb-10
WT	4.60	0.65	0.07	0.70	0.12	L452R	N	N	N	N	0.63
144Y del	52.56	9.17	0.15	3.00	1.86	Y453F	N	N	13.40	35.93	2.04
F338L	11.24	1.24	0.89	1.14	0.44	K458R	39.75	7.30	9.95	5.66	0.17
V341I	4.56	0.74	6.05	10.24	0.28	E471Q	77.40	38.15	9.89	3.17	6.08
F342L	23.04	3.79	6.43	5.71	1.21	I472V	0.69	0.24	17.24	0.42	0.80
A344S	4.75	55.23	0.78	0.54	6.67	G476S	N	4.47	10.72	13.57	0.38
A348S	5.58	1.25	0.11	5.37	0.18	S477N	1.38	0.19	1.25	0.68	1.08
A352S	61.14	16.26	37.31	13.38	1.35	S477R	163.70	45.37	3.76	3.66	6.39
N354D	154.60	1.50	0.70	1.46	0.21	T478I	7.09	66.40	12.94	4.23	3.70
S359N	1.93	2.81	0.33	1.40	0.13	P479S	273.00	3.12	9.24	40.93	10.30
V367F	25.31	2.26	26.57	6.87	0.93	G482S	3.42	0.64	0.26	1.05	14.26
N370S	2.55	14.14	4.87	1.51	2.95	V483I	7.36	0.76	0.40	1.63	3.39
F377L	4.65	1.91	23.93	0.37	18.12	V483A	71.67	4.83	13.11	17.46	1.91
K378R	2.45	0.91	0.39	1.64	7.70	E484Q	1.63	58.13	N	0.68	0.05
K378N	5.26	0.79	20.94	1.22	N	E484K	9.66	0.14	15.42	0.57	5.75
P384L	8.81	4.78	0.96	5.03	0.35	F490S	1.03	0.45	28.65	1.47	2.47
T385A	0.37	0.27	19.23	0.24	2.97	S494P	2.81	N	15.52	0.67	0.31
T393P	6.89	1.98	817.70	3.05	9.15	N501Y	N	14.67	19.73	N	2.72
V395I	0.26	0.29	2.09	1.16	0.58	V503F	64.82	35.13	2.63	0.73	1.60
E406Q	1.10	N	151.50	9.31	3.02	Y508H	99.92	17.02	5.18	3.90	6.96
R408I	271.20	13.69	2.04	2.18	0.10	A520S	137.60	10.04	9.26	1.25	2.15
Q409E	0.37	1.20	41.64	0.73	2.46	P521R	62.86	40.66	4.43	6.69	0.55
Q414E	1.09	1.45	1.59	2.27	0.90	P521S	245.30	17.75	1.96	1.81	3.53
K417T	7.96	0.37	1.98	0.78	2.11	A522S	38.24	6.31	3.83	1.22	1.20
K417N	5.19	5.80	0.14	2.60	2.10	A522V	57.89	36.13	25.34	8.91	0.09
A435S	415.70	5.93	2.74	20.34	4.99	D614G	267.80	7.78	14.66	0.76	0.89
N439K	17.74	5.07	94.07	12.61	0.50	P681H	4.51	72.64	4.50	0.63	0.27
N440K	155.00	1.04	18.80	61.88	12.78	T716I	27.99	3.44	0.05	0.63	0.46
K444R	173.70	0.45	49.44	4.90	1.98	S982A	92.86	10.36	1.51	2.54	0.14

[a]Nanobodies with NT_{50} values (μg/mL) greater than 15 μg/mL (1 μM) are highlighted in gray. N, neutralizing activity lost.

broad neutralization of variants. These attempts provide guidance for the rapid development of antibody therapeutics against emerging pathogens with highly variable characteristics.

The wide transmission and host adaptation of SARS-CoV-2 have led to the rapid accumulation of mutations, generating multiple circulating variants and subvariants. It has been reported that the recent Omicron subvariants BA.2.12.1, BA.4, and BA.5 have evolved mutations to escape from the humoral immunity elicited by the original Omicron BA.1 (42). Moreover, the recurrent spillovers of animal coronaviruses into the human population are becoming more frequent than previously thought (43). Broadly neutralizing antibodies that are not affected by ongoing antigenic drift and that can prevent or treat future zoonotic infections are urgently needed. The coronavirus RBD is one of the most effective NAb targets. However, our surface conservation mapping analysis indicates that the pan-sarbecovirus conserved epitopes are very limited, mainly focused on the RBD-6 community and part of RBD-7 (Fig. 1). It has been documented recently that the Spike fusion peptide is also a highly conserved candidate for next generation broad antibodies and vaccines (44). Therefore, it is extremely difficult to obtain pan-sarbecovirus NAbs through small sample size screening from convalescent patients.

In recent years, advances in computational structure-based antibody design have been made to improve antibody affinity and activity. Intensive research on SARS-CoV-2 has provided a wealth of useful structural biological information, including high-resolution antigen-antibody pairs. Paratope and epitope prediction (28), flexible or rigid protein docking (45), molecular dynamic simulation, deep learning (46), and neural networks were adopted for structure-guided antibody optimization for either COVID-19 or other diseases. However, computational design has been challenged and limited due to the lack of accuracy and iterative validation between wet and dry experiments. In this article, we tested the optimization potential of the RAbD framework in pan-sarbecovirus NAbs by sampling the diverse sequence, structure, and binding space of S2H97-RBD complexes, grafting structures from a set of canonical CDR clusters, and then redesigning multiple CDRs

with loops of different lengths, conformations, and sequences. Experimental data demonstrate that targeted optimization can indeed preserve and improve neutralizing activity, although design toward one particular variant may also result in a decrease in activity against some other variants. This may be because although the interacting amino acids within the RBD are highly conserved among sarbecoviruses, mutations at noninteracting sites may alter the overall flexibility of the RBD and lead to subtle conformational changes. These subtle dynamic alterations will affect the interacting amino acid side chain distance, force field, and free energy and consequently lead to the changes in affinity and activity. Interestingly, through recombination of the designed light chain and heavy chain, we were able to identify a new antibody, AI-1028, which showed improved and broadened neutralizing activity against multiple current SARS-CoV-2 variants (Omicron subvariants BA.5, XBB, BQ.1.1, and BA.2.3.20), clade 1a (SARS-CoV and WIV1), and clade 1b (bat RaTG13) sarbecoviruses. Regarding the mechanism, in the absence of direct evidence from the structural biology of the antigen-antibody complex, we can only speculate that the superior activity and broad spectrum demonstrated by the chimeric antibody AI-1028 might be due to the dynamic conformational change and complementary effects from the reconstitution of the two designed chains.

Here, we also identified two nanobodies with a relatively broad neutralizing spectrum. Bi-09 has a broader spectrum but relatively low activity; thus, it was engineered into a bivalent form. Monovalent Nb-10 showed high neutralizing activity against multiple tested sarbecoviruses except for Omicron variants. Although we have not had the chance to elucidate the structure and mechanism of these two nanobodies, their broad-spectrum characteristics suggest that they may recognize relatively conserved RBD epitopes. These two nanobodies can be designed for cocktail administration to limit resistance escape.

Given the high pandemic potential of zoonotic and epidemic sarbecoviruses, the development of countermeasures, such as pan-sarbecovirus antibodies, vaccines, and small molecule inhibitors, is a global health priority. One possible solution is to find NAbs by targeting evolutionarily conserved epitopes located outside the rapidly evolving RBM. This antibody would be anticipated to have a high barrier to resistance, and because of its nonoverlapping resistance profile, it could be combined with receptor-binding motif-targeted antibodies when necessary to further heighten the barrier to resistance. In addition, the pace of antibody drug development must be accelerated to address the rapid evolution of the virus. Our work offers the possibility of solving this problem through computational and synthetic biology.

MATERIALS AND METHODS

Cells and reagents. HEK293T (human kidney epithelial) cells were obtained from the China Infrastructure of Cell Line Resource (Beijing, China). The human hepatoma cell line Huh7 was obtained from Apath, Inc. (Brooklyn, NY, USA) with permission from Charles Rice (Rockefeller University). Expi293F cells, Gibco Expo293 Expression Medium, and the ExpiFectamine 293 Transfection kit were purchased from ThermoFisher (Waltham, MA, USA). The cells were maintained in Dulbecco's modified Eagle's medium (Thermo Fisher) supplemented with 2 to 10% fetal bovine serum (FBS; Thermo Fisher), nonessential amino acids, penicillin, and streptomycin. Recombinant RBD proteins were purchased from Sino Biological (Beijing, China). Horseradish peroxidase (HRP)/anti-CM13 monoclonal conjugate was purchased from GE Healthcare (Boston, MA, USA). AmMag Protein A Magnetic Beads were from GenScript (Nanjing, China).

Analysis of RBD sequence conservation. RBD amino acid sequence similarity was mapped onto the structure surface using the ConSurf web server (https://consurf.tau.ac.il/) (30). A clean RBD structure was prepared from the PDB file 7M7W and uploaded to the server. Furthermore, multiple sequence alignment (MSA) files containing multiple SARS-CoV-2 variants (Wuhan-Hu-1, Alpha, Beta, Gamma, Delta, Lambda, Kappa, Epsilon, Eta, Iota, Zeta, Omicron-BA.1, BA.2, BA.4, BA.5, BF.7, BQ.1.1, CA.3.1, CH.1.1, and XBB) or multiple sarbecoviruses (SARS-COV Tor2, WIV1, HKU3-1, RsSHC014, Rc-0319, GX-P4L, RaTG13, bat SARS-like coronavirus RsSHC014, YNLF_34C, Rs9401, SL_CoVZXC21, and SARS-COV-2 isolates as described above) were prepared in FASTA format and submitted online. PyMOL was used to generate, visualize, and create images of RBD evolutionary conservation patterns.

Computational design. RosettaAntibodyDesign (RAbD), a generalized framework for the design of antibodies, was used in this study to sample the diverse sequence, structure, and binding space of the S2H97/RBD complex (40). The starting antigen-antibody complex was obtained from the PDB file 7M7W and renumbered using PyIgClassify (19, 47). Before design calculations, the structure of 7M7W was minimized using the Rosetta energy function with Monte Carlo + minimization algorithms. A total of two antibody design strategies were used, where either $LCDR1^{+}LCDR2^{+}LCDR3$ or $HCDR1^{+}HCDR2$ were designed and the docking program was included. Both sequence_design and graft_design were applied. A total of 1,000 top decoys were output as separate Monte Carlo trajectories in parallel for each design strategy. Decoys were analyzed by the

Rosetta Feature reporter framework and ranked according to comprehensive scoring with the interface H-bonds number and dG_separated. Finally, 15 designed light chains and 20 designed heavy chains were adopted for full antibody expression, purification, and functional validation.

Nanobody selection by phage display. A synthetic nanobody phage display with high diversity was prepared by our laboratory as previously described (32, 35). To screen for broadly neutralizing nanobodies, three recombinant RBD proteins were used, and four rounds of panning were performed in both immunotubes and with magnetic bead-conjugated antigens. Briefly, for the second and fourth panning rounds, SARS-CoV RBD proteins were coated on Nunc MaxiSorp immunotubes (Thermo Fisher) at 5 μg/mL in PBS overnight. For the first and third panning rounds, SARS-CoV-2 variants Alpha or Omicron BA.5 RBD was first biotinylated with EZ-Link Sulfo-NHS-LCBiotin (Thermo Fisher) and then selected with streptavidin-coated magnetic Dynabeads M-280 (Thermo Fisher). Panning was performed following the standard procedure as previously described (32, 35). After biopanning, phage ELISA was performed with 480 individual colonies using anti-CM13 antibody (HRP) in plates coated with recombinant RBDs. The absorbance was measured using a SpectraMax M5 plate reader from Molecular Devices (San Jose, CA, USA). Positive clones were sent for sequencing, and after sequence alignments, distinct sequences were chosen for protein expression.

Expression and purification of nanobodies. The coding sequences of selected nanobodies were cloned into the pET22b plasmid by NcoI/XhoI for overexpression under the T7 promoter in *E. coli* BL21 (DE3). To improve the neutralization activity of nanobodies, we constructed bivalent Bi-09 with a $(GGGGS)_5$ linker introduced between the two monomers. Bacterial cultures were grown in LB media supplemented with 100 μg/mL ampicillin to an opitcal density at 600 nm of 0.6 to 0.8 in shaking incubators. Protein expression was induced by the addition of 0.5 mM IPTG followed by overnight incubation at 25°C. Proteins with a His tag fused to the C terminus were purified over Ni Sepharose 6 Fast Flow (GE Healthcare, Boston, MA, USA) and eluted with 300 mM imidazole. The expression and purification were verified using SDS-PAGE and subsequent Coomassie blue staining. Next, purified proteins were concentrated on filter tubes (Millipore, USA), and the elution buffer containing imidazole was exchanged with PBS (pH 7.4).

Expression and purification of human monoclonal antibodies. The heavy and light chain sequences of MAbs were synthesized by Tsingke Biotechnology Co., Ltd. (Beijing, China), cloned into mammalian expression plasmids under the control of the EF-α core promoter, and fused with the N-terminal interleukin-2 signal peptide. Maxiprepped plasmids were used for transfection, which was performed using ExpiFectamine 293 reagent (Thermo Fisher) according to the manufacturer's instructions. A final density of 2.5 to 3 $\times$ 10^6 viable cells/mL Exip293F (Thermo Fisher) was seeded 1 day before transfection. The next day, a transfection cocktail, formed at a ratio of 1.0 μg/mL:3.2 μL/mL (DNA:ExpiFectamine 293 Reagent), was diluted in Opti-MEM. After 20 min of incubation at room temperature, the mixture was transferred to the cells. At 18 to 22 h posttransfection, ExpiFectamine 293 Transfection Enhancer 1 and ExpiFectamine 293 Transfection Enhancer 2 were added to the transfection flask. Five days posttransfection, the proteins were harvested, purified by binding to AmMag Protein A Magnetic Beads (GenScript) and then eluted with 0.05 M citrate (pH 3.5). The expression and purification were verified using SDS-PAGE and subsequent Coomassie blue staining. Purified proteins were concentrated on filter tubes (Millipore, USA), and the elution buffer was exchanged with PBS (pH 7.4).

Plasmids, pseudovirus preparation, and neutralization assay. The pNL4.3-Luc-E-R- lentiviral vector has been reported in our previous publications (32). Briefly, the vector is in the HIV-1 pNL4-3 backbone with a deletion of Env and an addition of a Gaussia luciferase-reported gene that is expressed in target cells without premature expression in producer cells. The SARS-CoV spike gene was purchased from Sinobological (VG40150-G-N, Beijing, China). Codon-optimized spike genes of SARS-CoV-2 variants were synthesized by Rui Biotech (Beijing, China); alternatively, some of them were produced by PCR mutagenesis and then cloned into the pCAGGS vector through EcoRI and XhoI. The RaTG13 and WIV1 Spike genes were chemically synthesized by Rui Biotech. The profile of amino acid changes compared to the wild-type virus (GenBank QHD43416.1) for each variant is summarized in Table S2.

Pseudoviruses were produced in 293T cells by the cotransfection of Spike expression plasmids and pNL4.3-Luc-E-R- at a ratio of 1:1 with polyethyleneimine (transporter 5 transfection reagent; Polysciences). A nonenveloped lentivirus particle (bald virus) was also generated as a negative control. Six hours posttransfection, the medium was replaced with fresh medium and incubated for 48 h or 72 h. The culture supernatants containing pseudotyped viruses were harvested, and relative infectivity was determined by infection of Huh7 cells. The luciferase activity was measured 48 h postinfection.

Neutralization assays were performed as described previously (32, 35). The 10 times serially diluted antibodies were incubated with pseudotyped viruses at 37°C for 1 h. The mixture was subsequently incubated with Huh7 cells for 48 h. The cells were washed twice with PBS and lysed with lysis buffer before measuring luciferase activity. The neutralization titer was calculated as the antibody dilution at which the luciferase activity was reduced to 50% of that from the virus-only wells.

Affinity measurement and competition-binding study. Surface plasmon resonance experiments were performed as described previously (32). Recombinant RBD proteins were immobilized on CM5 sensor chips (GE Healthcare) at approximately 500 response units. For the affinity assays, nanobodies and monoantibodies were used as ligands and a series of dilutions flowed over the chip surface. After each cycle of association and dissociation, the chips were regenerated with glycine-HCl pH 2.5. Acquired data were analyzed with BIAevaluation software using a 1:1 binding model.

For competitive binding assays, the RBD protein was immobilized on the chip at approximately 300 response units. S2H97 and AI-1028 were diluted to a concentration of 25.6 nM in two separate cycles. S2H97 or IgG isotype antibody first flowed over the sensor surface for 500 s, and then AI-1028 flowed over without dissociation for another 500 s. The binding curves were analyzed with BIAevaluation software.

Statistics and reproducibility. Data were analyzed using GraphPad Prism 6.01 (GraphPad Software, San Diego, CA, USA). Antibody neutralization experiments usually use three to four duplicated wells for

each treatment. The infectivity data were first inversed to neutralization activity. Each neutralization data set was normalized by the background control (no virus) to define the real value for 100% neutralization. A four-parameter neutralization nonlinear regression model was fitted to report NT_{50} values. All experiments were performed independently at least twice, and similar results were obtained. Representative data from one experiment are shown.

SUPPLEMENTAL MATERIAL

Supplemental material is available online only.

SUPPLEMENTAL FILE 1, DOCX file, 0.5 MB.

ACKNOWLEDGMENTS

This work was supported by National Natural Science Foundation of China (U22A20553 and 82241064) and Chinese Academy of Medical Sciences (CAMS) Innovation Fund for Medical Sciences (2021-I2M-1-038 and 2022-I2M-1-021).

We declare no conflict of interest.

REFERENCES

1. DeGrace MM, Ghedin E, Frieman MB, Krammer F, Grifoni A, Alisoltani A, Alter G, Amara RR, Baric RS, Barouch DH, Bloom JD, Bloyet LM, Bonenfant G, Boon ACM, Boritz EA, Bratt DL, Bricker TL, Brown L, Buchser WJ, Carreno JM, Cohen-Lavi L, Darling TL, Davis-Gardner ME, Dearlove BL, Di H, Dittmann M, Doria-Rose NA, Douek DC, Drosten C, Edara VV, Ellebedy A, Fabrizio TP, Ferrari G, Fischer WM, Florence WC, Fouchier RAM, Franks J, Garcia-Sastre A, Godzik A, Gonzalez-Reiche AS, Gordon A, Haagmans BL, Halfmann PJ, Ho DD, Holbrook MR, Huang Y, James SL, Jaroszewski L, Jeevan T, Johnson RM, et al. 2022. Defining the risk of SARS-CoV-2 variants on immune protection. Nature 605:640–652. https://doi.org/10.1038/s41586-022-04690-5.
2. Coronaviridae Study Group of the International Committee on Taxonomy of Viruses. 2020. The species severe acute respiratory syndrome-related coronavirus: classifying 2019-nCoV and naming it SARS-CoV-2. Nat Microbiol 5:536–544. https://doi.org/10.1038/s41564-020-0695-z.
3. Cui J, Li F, Shi ZL. 2019. Origin and evolution of pathogenic coronaviruses. Nat Rev Microbiol 17:181–192. https://doi.org/10.1038/s41579-018-0118-9.
4. Forni D, Cagliani R, Clerici M, Sironi M. 2017. Molecular evolution of human coronavirus genomes. Trends Microbiol 25:35–48. https://doi.org/10.1016/j.tim.2016.09.001.
5. Zhou P, Yang XL, Wang XG, Hu B, Zhang L, Zhang W, Si HR, Zhu Y, Li B, Huang CL, Chen HD, Chen J, Luo Y, Guo H, Jiang RD, Liu MQ, Chen Y, Shen XR, Wang X, Zheng XS, Zhao K, Chen QJ, Deng F, Liu LL, Yan B, Zhan FX, Wang YY, Xiao GF, Shi ZL. 2020. A pneumonia outbreak associated with a new coronavirus of probable bat origin. Nature 579:270–273. https://doi.org/10.1038/s41586-020-2012-7.
6. Li W, Shi Z, Yu M, Ren W, Smith C, Epstein JH, Wang H, Crameri G, Hu Z, Zhang H, Zhang J, McEachern J, Field H, Daszak P, Eaton BT, Zhang S, Wang LF. 2005. Bats are natural reservoirs of SARS-like coronaviruses. Science 310:676–679. https://doi.org/10.1126/science.1118391.
7. Li D, Sempowski GD, Saunders KO, Acharya P, Haynes BF. 2022. SARS-CoV-2 neutralizing antibodies for COVID-19 prevention and treatment. Annu Rev Med 73:1–16. https://doi.org/10.1146/annurev-med-042420-113838.
8. Ju B, Zhang Q, Ge J, Wang R, Sun J, Ge X, Yu J, Shan S, Zhou B, Song S, Tang X, Yu J, Lan J, Yuan J, Wang H, Zhao J, Zhang S, Wang Y, Shi X, Liu L, Zhao J, Wang X, Zhang Z, Zhang L. 2020. Human neutralizing antibodies elicited by SARS-CoV-2 infection. Nature 584:115–119. https://doi.org/10.1038/s41586-020-2380-z.
9. Barnes CO, Jette CA, Abernathy ME, Dam KA, Esswein SR, Gristick HB, Malyutin AG, Sharaf NG, Huey-Tubman KE, Lee YE, Robbiani DF, Nussenzweig MC, West AP, Jr, Bjorkman PJ. 2020. SARS-CoV-2 neutralizing antibody structures inform therapeutic strategies. Nature 588:682–687. https://doi.org/10.1038/s41586-020-2852-1.
10. Corti D, Purcell LA, Snell G, Veesler D. 2021. Tackling COVID-19 with neutralizing monoclonal antibodies. Cell 184:3086–3108. https://doi.org/10.1016/j.cell.2021.05.005.
11. Xiang Y, Nambulli S, Xiao Z, Liu H, Sang Z, Duprex WP, Schneidman-Duhovny D, Zhang C, Shi Y. 2020. Versatile and multivalent nanobodies efficiently neutralize SARS-CoV-2. Science 370:1479–1484. https://doi.org/10.1126/science.abe4747.
12. Fang Y, Sun P, Xie X, Du M, Du F, Ye J, Kalveram BK, Plante JA, Plante KS, Li B, Bai XC, Shi PY, Chen ZJ. 2022. An antibody that neutralizes SARS-CoV-1 and SARS-CoV-2 by binding to a conserved spike epitope outside the receptor binding motif. Sci Immunol 7:eabp9962. https://doi.org/10.1126/sciimmunol.abp9962.
13. Ge XY, Li JL, Yang XL, Chmura AA, Zhu G, Epstein JH, Mazet JK, Hu B, Zhang W, Peng C, Zhang YJ, Luo CM, Tan B, Wang N, Zhu Y, Crameri G, Zhang SY, Wang LF, Daszak P, Shi ZL. 2013. Isolation and characterization of a bat SARS-like coronavirus that uses the ACE2 receptor. Nature 503:535–538. https://doi.org/10.1038/nature12711.
14. Liu K, Pan X, Li L, Yu F, Zheng A, Du P, Han P, Meng Y, Zhang Y, Wu L, Chen Q, Song C, Jia Y, Niu S, Lu D, Qiao C, Chen Z, Ma D, Ma X, Tan S, Zhao X, Qi J, Gao GF, Wang Q. 2021. Binding and molecular basis of the bat coronavirus RaTG13 virus to ACE2 in humans and other species. Cell 184:3438–3451.e10. https://doi.org/10.1016/j.cell.2021.05.031.
15. Jackson CB, Farzan M, Chen B, Choe H. 2022. Mechanisms of SARS-CoV-2 entry into cells. Nat Rev Mol Cell Biol 23:3–20. https://doi.org/10.1038/s41580-021-00418-x.
16. Shi R, Shan C, Duan X, Chen Z, Liu P, Song J, Song T, Bi X, Han C, Wu L, Gao G, Hu X, Zhang Y, Tong Z, Huang W, Liu WJ, Wu G, Zhang B, Wang L, Qi J, Feng H, Wang FS, Wang Q, Gao GF, Yuan Z, Yan J. 2020. A human neutralizing antibody targets the receptor-binding site of SARS-CoV-2. Nature 584:120–124. https://doi.org/10.1038/s41586-020-2381-y.
17. Baum A, Ajithdoss D, Copin R, Zhou A, Lanza K, Negron N, Ni M, Wei Y, Mohammadi K, Musser B, Atwal GS, Oyejide A, Goez-Gazi Y, Dutton J, Clemmons E, Staples HM, Bartley C, Klaffke B, Alfson K, Gazi M, Gonzalez O, Dick E, Jr, Carrion R, Jr, Pessaint L, Porto M, Cook A, Brown R, Ali V, Greenhouse J, Taylor T, Andersen H, Lewis MG, Stahl N, Murphy AJ, Yancopoulos GD, Kyratsous CA. 2020. REGN-COV2 antibodies prevent and treat SARS-CoV-2 infection in rhesus macaques and hamsters. Science 370:1110–1115. https://doi.org/10.1126/science.abe2402.
18. Pinto D, Park YJ, Beltramello M, Walls AC, Tortorici MA, Bianchi S, Jaconi S, Culap K, Zatta F, De Marco A, Peter A, Guarino B, Spreafico R, Cameroni E, Case JB, Chen RE, Havenar-Daughton C, Snell G, Telenti A, Virgin HW, Lanzavecchia A, Diamond MS, Fink K, Veesler D, Corti D. 2020. Cross-neutralization of SARS-CoV-2 by a human monoclonal SARS-CoV antibody. Nature 583:290–295. https://doi.org/10.1038/s41586-020-2349-y.
19. Starr TN, Czudnochowski N, Liu Z, Zatta F, Park YJ, Addetia A, Pinto D, Beltramello M, Hernandez P, Greaney AJ, Marzi R, Glass WG, Zhang I, Dingens AS, Bowen JE, Tortorici MA, Walls AC, Wojcechowskyj JA, De Marco A, Rosen LE, Zhou J, Montiel-Ruiz M, Kaiser H, Dillen JR, Tucker H, Bassi J, Silacci-Fregni C, Housley MP, di Iulio J, Lombardo G, Agostini M, Sprugasci N, Culap K, Jaconi S, Meury M, Dellota E, Jr, Abdelnabi R, Foo SC, Cameroni E, Stumpf S, Croll TI, Nix JC, Havenar-Daughton C, Piccoli L, Benigni F, Neyts J, Telenti A, Lempp FA, Pizzuto MS, Chodera JD, et al. 2021. SARS-CoV-2 RBD antibodies that maximize breadth and resistance to escape. Nature 597:97–102. https://doi.org/10.1038/s41586-021-03807-6.
20. Yuan M, Wu NC, Zhu X, Lee CD, So RTY, Lv H, Mok CKP, Wilson IA. 2020. A highly conserved cryptic epitope in the receptor binding domains of SARS-CoV-2 and SARS-CoV. Science 368:630–633. https://doi.org/10.1126/science.abb7269.
21. Park YJ, De Marco A, Starr TN, Liu Z, Pinto D, Walls AC, Zatta F, Zepeda SK, Bowen JE, Sprouse KR, Joshi A, Giurdanella M, Guarino B, Noack J, Abdelnabi R, Foo SC, Rosen LE, Lempp FA, Benigni F, Snell G, Neyts J, Whelan SPJ, Virgin HW, Bloom JD, Corti D, Pizzuto MS, Veesler D. 2022. Antibody-mediated broad sarbecovirus neutralization through ACE2 molecular mimicry. Science 375:449–454. https://doi.org/10.1126/science.abm8143.

22. Tortorici MA, Beltramello M, Lempp FA, Pinto D, Dang HV, Rosen LE, McCallum M, Bowen J, Minola A, Jaconi S, Zatta F, De Marco A, Guarino B, Bianchi S, Lauron EJ, Tucker H, Zhou J, Peter A, Havenar-Daughton C, Wojcechowskyj JA, Case JB, Chen RE, Kaiser H, Montiel-Ruiz M, Meury M, Czudnochowski N, Spreafico R, Dillen J, Ng C, Sprugasci N, Culap K, Benigni F, Abdelnabi R, Foo SC, Schmid MA, Cameroni E, Riva A, Gabrieli A, Galli M, Pizzuto MS, Neyts J, Diamond MS, Virgin HW, Snell G, Corti D, Fink K, Veesler D. 2020. Ultrapotent human antibodies protect against SARS-CoV-2 challenge via multiple mechanisms. Science 370:950–957. https://doi.org/10.1126/science.abe3354.
23. Tortorici MA, Czudnochowski N, Starr TN, Marzi R, Walls AC, Zatta F, Bowen JE, Jaconi S, Di Iulio J, Wang Z, De Marco A, Zepeda SK, Pinto D, Liu Z, Beltramello M, Bartha I, Housley MP, Lempp FA, Rosen LE, Dellota E, Jr, Kaiser H, Montiel-Ruiz M, Zhou J, Addetia A, Guarino B, Culap K, Sprugasci N, Saliba C, Vetti E, Giacchetto-Sasselli I, Fregni CS, Abdelnabi R, Foo SC, Havenar-Daughton C, Schmid MA, Benigni F, Cameroni E, Neyts J, Telenti A, Virgin HW, Whelan SPJ, Snell G, Bloom JD, Corti D, Veesler D, Pizzuto MS. 2021. Broad sarbecovirus neutralization by a human monoclonal antibody. Nature 597:103–108. https://doi.org/10.1038/s41586-021-03817-4.
24. Wang Y, Liu M, Shen Y, Ma Y, Li X, Zhang Y, Liu M, Yang XL, Chen J, Yan R, Luan D, Wang Y, Chen Y, Wang Q, Lin H, Li Y, Wu K, Zhu T, Zhao J, Lu H, Wen Y, Jiang S, Wu F, Zhou Q, Shi ZL, Huang J. 2022. Novel sarbecovirus bispecific neutralizing antibodies with exceptional breadth and potency against currently circulating SARS-CoV-2 variants and sarbecoviruses. Cell Discov 8:36. https://doi.org/10.1038/s41421-022-00401-6.
25. Wang P, Casner RG, Nair MS, Yu J, Guo Y, Wang M, Chan JF, Cerutti G, Iketani S, Liu L, Sheng Z, Chen Z, Yuen KY, Kwong PD, Huang Y, Shapiro L, Ho DD. 2022. A monoclonal antibody that neutralizes SARS-CoV-2 variants, SARS-CoV, and other sarbecoviruses. Emerg Microbes Infect 11:147–157. https://doi.org/10.1080/22221751.2021.2011623.
26. Tunyasuvunakool K, Adler J, Wu Z, Green T, Zielinski M, Zidek A, Bridgland A, Cowie A, Meyer C, Laydon A, Velankar S, Kleywegt GJ, Bateman A, Evans R, Pritzel A, Figurnov M, Ronneberger O, Bates R, Kohl SAA, Potapenko A, Ballard AJ, Romera-Paredes B, Nikolov S, Jain R, Clancy E, Reiman D, Petersen S, Senior AW, Kavukcuoglu K, Birney E, Kohli P, Jumper J, Hassabis D. 2021. Highly accurate protein structure prediction for the human proteome. Nature 596:590–596. https://doi.org/10.1038/s41586-021-03828-1.
27. AlQuraishi M. 2021. Machine learning in protein structure prediction. Curr Opin Chem Biol 65:1–8. https://doi.org/10.1016/j.cbpa.2021.04.005.
28. Pittala S, Bailey-Kellogg C. 2020. Learning context-aware structural representations to predict antigen and antibody binding interfaces. Bioinformatics 36:3996–4003. https://doi.org/10.1093/bioinformatics/btaa263.
29. Shan S, Luo S, Yang Z, Hong J, Su Y, Ding F, Fu L, Li C, Chen P, Ma J, Shi X, Zhang Q, Berger B, Zhang L, Peng J. 2022. Deep learning guided optimization of human antibody against SARS-CoV-2 variants with broad neutralization. Proc Natl Acad Sci U S A 119:e2122954119. https://doi.org/10.1073/pnas.2122954119.
30. Ashkenazy H, Abadi S, Martz E, Chay O, Mayrose I, Pupko T, Ben-Tal N. 2016. ConSurf 2016: an improved methodology to estimate and visualize evolutionary conservation in macromolecules. Nucleic Acids Res 44:W344–50. https://doi.org/10.1093/nar/gkw408.
31. Prassler J, Thiel S, Pracht C, Polzer A, Peters S, Bauer M, Norenberg S, Stark Y, Kolln J, Popp A, Urlinger S, Enzelberger M. 2011. HuCAL PLATINUM, a synthetic Fab library optimized for sequence diversity and superior performance in mammalian expression systems. J Mol Biol 413:261–278. https://doi.org/10.1016/j.jmb.2011.08.012.
32. Chi X, Liu X, Wang C, Zhang X, Li X, Hou J, Ren L, Jin Q, Wang J, Yang W. 2020. Humanized single domain antibodies neutralize SARS-CoV-2 by targeting the spike receptor binding domain. Nat Commun 11:4528. https://doi.org/10.1038/s41467-020-18387-8.
33. Larios Mora A, Detalle L, Gallup JM, Van Geelen A, Stohr T, Duprez L, Ackermann MR. 2018. Delivery of ALX-0171 by inhalation greatly reduces respiratory syncytial virus disease in newborn lambs. MAbs 10:778–795. https://doi.org/10.1080/19420862.2018.1470727.
34. Hamers-Casterman C, Atarhouch T, Muyldermans S, Robinson G, Hamers C, Songa EB, Bendahman N, Hamers R. 1993. Naturally occurring antibodies devoid of light chains. Nature 363:446–448. https://doi.org/10.1038/363446a0.
35. Chi X, Zhang X, Pan S, Yu Y, Shi Y, Lin T, Duan H, Liu X, Chen W, Yang X, Chen L, Dong X, Ren L, Ding Q, Wang J, Yang W. 2022. An ultrapotent RBD-targeted biparatopic nanobody neutralizes broad SARS-CoV-2 variants. Signal Transduct Target Ther 7:44. https://doi.org/10.1038/s41392-022-00912-4.
36. Koenig PA, Das H, Liu H, Kummerer BM, Gohr FN, Jenster LM, Schiffelers LDJ, Tesfamariam YM, Uchima M, Wuerth JD, Gatterdam K, Ruetalo N, Christensen MH, Fandrey CI, Normann S, Todtmann JMP, Pritzl S, Hanke L, Boos J, Yuan M, Zhu X, Schmid-Burgk JL, Kato H, Schindler M, Wilson IA, Geyer M, Ludwig KU, Hallberg BM, Wu NC, Schmidt FI. 2021. Structure-guided multivalent nanobodies block SARS-CoV-2 infection and suppress mutational escape. Science 371:eabe6230. https://doi.org/10.1126/science.abe6230.
37. Aria H, Mahmoodi F, Ghaheh HS, Faranak M, Zare H, Heiat M, Bakherad H. 2022. Outlook of therapeutic and diagnostic competency of nanobodies against SARS-CoV-2: a systematic review. Anal Biochem 640:114546. https://doi.org/10.1016/j.ab.2022.114546.
38. Wells HL, Letko M, Lasso G, Ssebide B, Nziza J, Byarugaba DK, Navarrete-Macias I, Liang E, Cranfield M, Han BA, Tingley MW, Diuk-Wasser M, Goldstein T, Johnson CK, Mazet JAK, Chandran K, Munster VJ, Gilardi K, Anthony SJ. 2021. The evolutionary history of ACE2 usage within the coronavirus subgenus Sarbecovirus. Virus Evol 7:veab007. https://doi.org/10.1093/ve/veab007.
39. Hastie KM, Li H, Bedinger D, Schendel SL, Dennison SM, Li K, Rayaprolu V, Yu X, Mann C, Zandonatti M, Diaz Avalos R, Zyla D, Buck T, Hui S, Shaffer K, Hariharan C, Yin J, Olmedillas E, Enriquez A, Parekh D, Abraha M, Feeney E, Horn GQ, Aldon Y, Ali H, Aracic S, Cobb RR, Federman RS, Fernandez JM, Glanville J, Green R, Grigoryan G, Lujan Hernandez AG, Ho DD, Huang K-YA, Ingraham J, Jiang W, Kellam P, Kim C, Kim M, Kim HM, Kong C, Krebs SJ, Lan F, Lang G, Lee S, Leung CL, Liu J, Lu Y, MacCamy A, CoVIC-DB team1, et al. 2021. Defining variant-resistant epitopes targeted by SARS-CoV-2 antibodies: a global consortium study. Science 374:472–478. https://doi.org/10.1126/science.abh2315.
40. Adolf-Bryfogle J, Kalyuzhniy O, Kubitz M, Weitzner BD, Hu X, Adachi Y, Schief WR, Dunbrack RL, Jr, 2018. RosettaAntibodyDesign (RAbD): a general framework for computational antibody design. PLoS Comput Biol 14:e1006112. https://doi.org/10.1371/journal.pcbi.1006112.
41. Schoof M, Faust B, Saunders RA, Sangwan S, Rezelj V, Hoppe N, Boone M, Billesbolle CB, Puchades C, Azumaya CM, Kratochvil HT, Zimanyi M, Deshpande I, Liang J, Dickinson S, Nguyen HC, Chio CM, Merz GE, Thompson MC, Diwanji D, Schaefer K, Anand AA, Dobzinski N, Zha BS, Simoneau CR, Leon K, White KM, Chio US, Gupta M, Jin M, Li F, Liu Y, Zhang K, Bulkley D, Sun M, Smith AM, Rizo AN, Moss F, Brilot AF, Pourmal S, Trenker R, Pospiech T, Gupta S, Barsi-Rhyne B, Belyy V, Barile-Hill AW, Nock S, Liu Y, Krogan NJ, Ralston CY, QCRG Structural Biology Consortium, et al. 2020. An ultrapotent synthetic nanobody neutralizes SARS-CoV-2 by stabilizing inactive Spike. Science 370:1473–1479. https://doi.org/10.1126/science.abe3255.
42. Cao Y, Yisimayi A, Jian F, Song W, Xiao T, Wang L, Du S, Wang J, Li Q, Chen X, Yu Y, Wang P, Zhang Z, Liu P, An R, Hao X, Wang Y, Wang J, Feng R, Sun H, Zhao L, Zhang W, Zhao D, Zheng J, Yu L, Li C, Zhang N, Wang R, Niu X, Yang S, Song X, Chai Y, Hu Y, Shi Y, Zheng L, Li Z, Gu Q, Shao F, Huang W, Jin R, Shen Z, Wang Y, Wang X, Xiao J, Xie XS. 2022. BA.2.12.1, BA.4 and BA.5 escape antibodies elicited by Omicron infection. Nature 608:593–602. https://doi.org/10.1038/s41586-022-04980-y.
43. Lednicky JA, Tagliamonte MS, White SK, Elbadry MA, Alam MM, Stephenson CJ, Bonny TS, Loeb JC, Telisma T, Chavannes S, Ostrov DA, Mavian C, Beau De Rochars VM, Salemi M, Morris JG Jr. 2021. Independent infections of porcine deltacoronavirus among Haitian children. Nature 600:133–137. https://doi.org/10.1038/s41586-021-04111-z.
44. Dacon C, Tucker C, Peng L, Lee CD, Lin TH, Yuan M, Cong Y, Wang L, Purser L, Williams JK, Pyo CW, Kosik I, Hu Z, Zhao M, Mohan D, Cooper AJR, Peterson M, Skinner J, Dixit S, Kollins E, Huzella L, Perry D, Byrum R, Lembirik S, Drawbaugh D, Eaton B, Zhang Y, Yang ES, Chen M, Leung K, Weinberg RS, Pegu A, Geraghty DE, Davidson E, Douagi I, Moir S, Yewdell JW, Schmaljohn C, Crompton PD, Holbrook MR, Nemazee D, Mascola JR, Wilson IA, Tan J. 2022. Broadly neutralizing antibodies target the coronavirus fusion peptide. Science 377:728–735. https://doi.org/10.1126/science.abq3773.
45. Norman RA, Ambrosetti F, Bonvin A, Colwell LJ, Kelm S, Kumar S, Krawczyk K. 2020. Computational approaches to therapeutic antibody design: established methods and emerging trends. Brief Bioinform 21:1549–1567. https://doi.org/10.1093/bib/bbz095.
46. Schneider C, Buchanan A, Taddese B, Deane CM. 2022. DLAB: deep learning methods for structure-based virtual screening of antibodies. Bioinformatics 38:377–383. https://doi.org/10.1093/bioinformatics/btab660.
47. Adolf-Bryfogle J, Xu Q, North B, Lehmann A, Dunbrack RL, Jr, 2015. PyIgClassify: a database of antibody CDR structural classifications. Nucleic Acids Res 43:D432–8. https://doi.org/10.1093/nar/gku1106.